

Brookite titania photocatalytic nanomaterials: Synthesis, properties, and applications*

Jimin Xie[‡], Xiaomeng Lü, Jun Liu, and Huoming Shu

School of Chemistry and Chemical Engineering, Jiangsu University, 212013
Zhenjiang, China

Abstract: Phase-pure brookite TiO₂ and its activity has been obscured for its difficulty of synthesis. Hence, we introduced the method of preparation and property of phase-pure brookite TiO₂ and prepared phase-pure brookite TiO₂ by hydrothermal method using Ti(SO₄)₂ as precursor. Phase formation was achieved by hydrothermal treatment at 180 °C after different synthesis time. The physical and photophysical properties of samples were characterized by X-ray diffraction (XRD), transmission electron microscopy (TEM), UV–vis diffraction (UV–vis/DRS), and Raman spectroscopy. The dependence of the photocatalytic activities on synthesis time and correlations with the physical properties of brookite samples was examined in detail. In the case of mineralization of rhodamine B (Rh B), the sample with the narrowest bandgap and the lowest photoluminescence (PL) intensity (at hydrothermal synthesis time 36 h) showed the best photodecolorization activity. Proposed decolorization mechanism was elucidated in the light of the UV–vis spectra of the analyzed degradation products and frontier electron density (FED) theory. The results indicated that photocatalytic decolorization by brookite TiO₂ is a highly effective way to remove Rh B under near-visible light irradiation.

Keywords: brookite; particle synthesis; photodecolorization; photodegradation; rhodamine B; sampling.

INTRODUCTION

Titania (TiO₂) is an important functional inorganic material and exists in three main phases: anatase, brookite, and rutile [1]. The rutile and anatase phases have been widely investigated for their synthesis and application [2–8], while limited work has been done on brookite. Brookite has been reported to be difficult to prepare without any anatase or rutile phase, which limit its study and application [9]. However, compared with anatase and rutile, brookite has many sole properties [10,11]. Brookite is of lower symmetry and orthorhombic structure with six different nearest-neighbor Ti–O bond lengths, values of which span a larger range than in the tetragonal forms. Hence, brookite has only minor effects on the generation of charge carriers and on the shape of the photoaction spectra when it is used in photocells and is a good candidate for photovoltaic devices. Density functional theory calculations have been performed to determine the different structures and reactivities of TiO₂ polymorphs, results of which indicated that brookite (210) would exhibit distinct activity and may be useful in catalytic and photocatalytic applications [12]. Moreover, it has been found to exhibit higher activity than rutile and anatase

*Paper based on a presentation at the International Symposium on Novel Materials and their Synthesis (NMS-IV) and the 18th International Symposium on Fine Chemistry and Functional Polymers (FCFP-XVIII), 15–18 October 2008, Zhenjiang, China. Other presentations are published in this issue, pp. 2253–2424.

[‡]Corresponding author

in photocatalysis and catalytic reactions involving TiO₂-supported metal clusters in a few cases [13–15].

Presently, efficient schemes to synthesize brookite with high purity have been devised, generating more and more interest in the physicochemical properties and possible applications of this TiO₂ polymorph. Showa Denko K.K. (SDK) of Japan has announced development of a new photocatalyst responsive to visible light, using brookite nanoparticles [16]. With applications spread widely, brookite is expected to increase. This, in turn, requires good knowledge about the structural evolution accompanying the preparation method. However, owing to the relatively low thermodynamical stability for brookite, reaction conditions that can guarantee both selective nanocrystal nucleation and growth in this crystal phase are inherently more restrictive than those required for obtaining either anatase or rutile. As a matter of fact, conventional aqueous precipitation frequently yield brookite as a minor byproduct, while a number of experimental variables (e.g., water to precursor ratio, solution pH, and reaction temperature) need to be delicately adjusted in order to increase phase selectivity, however, at the cost of reproducibility.

Recently, many preparation methods of TiO₂ have been widely investigated, among which hydrothermal treatment has been drawing much attention considering that it directly produces well-crystallized nanocrystallites of a wide range of compositions within a short period of reaction time [17]. Pure brookite via hydrothermal treatment was previously obtained at high temperature (such as 300 °C) [18]. Recently, Kakihana et al. have reported synthesis of single-phase TiO₂ by varying the ligand in the water-soluble Ti complex and pH of the aqueous solution, among which glycolate acid was used for the synthesis of pure brookite TiO₂ by a hydrothermal method under high pH conditions. The vessel with precursor was heated at 200 °C for 24 h [19]. Ohno et al. prepared single-phase brookite TiO₂ by hydrothermal treatment of titanate nanotubes under perchloric acidic solution. The reaction was conducted at 200 °C for 50 h [20]. Since the preparation of pure brookite TiO₂ involves the complex reactant or harsh conditions, this has prompted us to investigate whether pure brookite could be obtained by a simple hydrothermal approach.

In this study, we prepared phase-pure brookite via a relatively simple hydrothermal method. Ti(SO₄)₂, which is easily manipulable, has been used in this study as a Ti source for synthesis. The structure and photoabsorption properties of the prepared samples were characterized in detail by combined means of X-ray diffraction (XRD), Raman spectroscopy, and UV–vis spectroscopy. The photocatalytic activity of brookite was investigated via bleaching rhodamine B (Rh B) under iodine tungsten lamp irradiation. The mechanism of Rh B photocatalytic decolorization was studied not only experimentally but also theoretically by calculating the frontier electron density (FED) of Rh B using Gaussian 03 soft package [21].

EXPERIMENTAL

Nanoparticle synthesis

All chemicals used in this study were analytical grade and were used without further purification. Distilled water was used in all experiments. Six sets of samples were prepared at different hydrothermal synthesis time to compare the structure and crystallinity of the particles. In the present study, Ti(SO₄)₂ was used as precursor, which was hydrolyzed using 2 mol⁻¹ NaOH. The subsequent collected precipitate was then transferred into six Teflon-lined autoclaves, which was then sealed into a stainless steel tank for hydrothermal treatment at 180 °C. The studied hydrothermal time were 2, 12, 24, 36, 48, and 60 h, respectively. Then the reactor was cooled to room temperature naturally, and the resulted product was collected and washed with deionized water and dried at 80 °C in air.

Characterization techniques

Purity and crystallization of the samples were characterized by powder XRD on a D/max-γA X-ray spectrometer (Rigaku, Japan) at 40 kV and 200 mA with monochromatic Cu Kα ($\lambda = 1.5418 \text{ \AA}$) radiation. Transmission electron microscopy (TEM) images were taken on a TECNAI12 TEM instrument (Philips) UV-vis diffuse reflectance spectra of the samples were measured by using a UV-2401 (Shimadzu) UV-vis spectrophotometer. The photoluminescence (PL) spectra were obtained by using a Cary Eclipse Scanning UV-vis system (Varian) equipped with sphere diffuse reflectance accessory. The Raman spectra were recorded by a Renishaw spectrometer (in Via) operating at 532 nm.

Photocatalytic evaluation

A 200-W iodine tungsten lamp was used in the photocatalytic experiments, which was placed in a cooling trap for maintaining the constant temperature by water circulation. Aqueous solution of Rh B with brookite sample was placed in photochemical reactor and purged with air at a fixed flow rate throughout the experiments. The solutions with samples were equilibrated in the dark for 20 min before irradiation. Samples were collected per 30 min and centrifuged for UV-vis analysis.

Quantum calculation

Quantum calculation using a Gaussian 03 program was carried out to get the frontier electronic density of Rh B. The calculated geometries of Rh B were fully optimized using hybrid density functional B3LYP with the 6-31G (d) basis set. The highest occupied molecular orbital (HOMO) and lowest unoccupied molecular orbital (LUMO) electron densities for every atom of Rh B were calculated on the base of the fully optimized geometries of Rh B. According to the frontier MO theory, for a radical reaction, the point of attack is at the position where the highest density of the sum of each electron occurs when they are in the HOMO and LUMO, respectively. The FED (f_x) can be calculated as

$$f_r = \sum_i (C_{ri}^{\text{HOMO}})^2 + (C_{ri}^{\text{LUMO}})^2 \quad (1)$$

where C_{ri}^{HOMO} and C_{ri}^{LUMO} are the coefficients of the atomic orbital in the HOMO and LUMO, respectively and r is the number of atom orbitals.

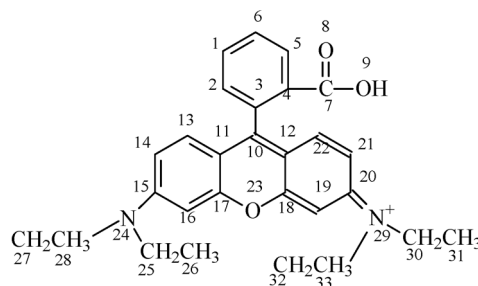


Fig. 1 Molecular structure of Rh B.

Table 1 MO calculations of electron densities and point charges for Rh B in water phase.

Atom number	Atom type	Electron density
1	C	0.0054
2	C	0.012
3	C	0.0017
4	C	0.013
5	C	0.004
6	C	0.0002
7	C	0.002
8	O	0.017
9	O	0.0005
10	C	0.15
11	C	0.1
12	C	0.099
13	C	0.14
14	C	0.079
15	C	0.05
16	C	0.025
17	C	0.045
18	C	0.009
19	C	0.012
20	C	0.159
21	C	0.087
22	C	0.14
23	O	0.025
24	N	0.19
25	C	0.0003
26	C	0.0005
27	C	0.004
28	C	0.001
29	N	0.17
30	C	0.004
31	C	0.02
32	C	0.003
33	C	0.03

RESULTS AND DISCUSSION

Figure 2 shows XRD patterns of samples prepared at different hydrothermal times, which greatly influence the structure of samples. Sample (2 h) was partly crystallized and tended to perfect crystallite with the increase of hydrothermal time. Sample (24 h) was phase-pure brookite TiO_2 (JCPDS card no.: 12-1360). Increasing the hydrothermal time produced enhancement in crystallinity of pure brookite, as evidenced by an increase in the sharpness and intensity of reflection at $2\theta = 32.8^\circ$.

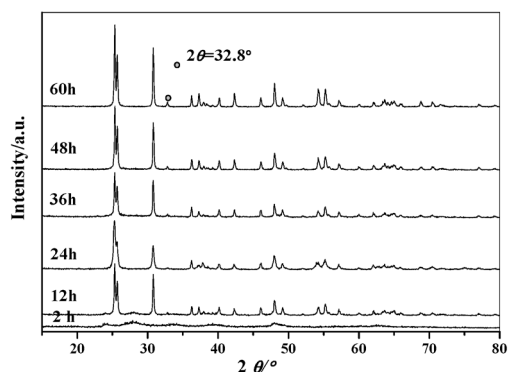


Fig. 2 XRD pattern of samples prepared at different hydrothermal times.

The Raman spectra of four crystalline samples were compared in Fig. 3. Brookite samples were characterized by a relatively complex vibration spectrum when compared with other polymorphs of TiO₂. All of the peaks are consistent with Raman spectrum of natural brookite TiO₂, except the absence of two weak peaks. In total, 14 bands were identified, including five A_{1g} (155, 195, 247, 414, 636 cm⁻¹), four B_{1g} (215, 323, 414, 503 cm⁻¹), four B_{2g} (366, 394, 462, 585 cm⁻¹), and B_{3g} (287 cm⁻¹).

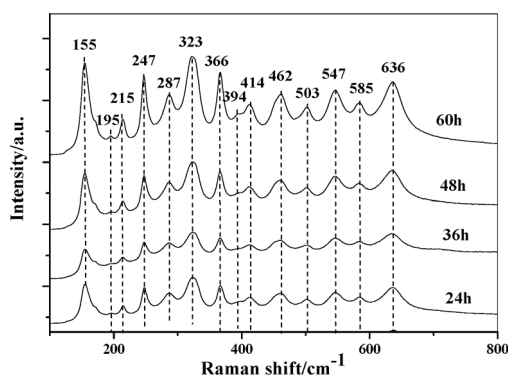


Fig. 3 Raman spectra of samples prepared at different hydrothermal times.

TiO₂ is known to be an indirect semiconductor. The relation between absorbance (A) and the incident photoenergy ($h\nu$) can be written as

$$A = C (h\nu - E_g)^{1/2}/h\nu \quad (2)$$

where C is the coefficient of proportionality, A is absorbance, h is the Plank constant, and E_g is bandgap. Plots of $(Ah\nu)^2$ vs. $h\nu$ are presented in Fig. 4. Extrapolating the linear part of the curve for different samples gives E_g . The bandgap was calculated to be 3.18 eV (12 h), 3.12 eV (24 h), 3.09 eV (36 h), 3.18 eV (48 h), and 3.13 eV (60 h). The optical bandgaps of anatase and rutile have been widely reported, i.e., ~3.2 eV for anatase and 3.0 eV for rutile. Hence, the value of brookite samples falls in between those of anatase and rutile.

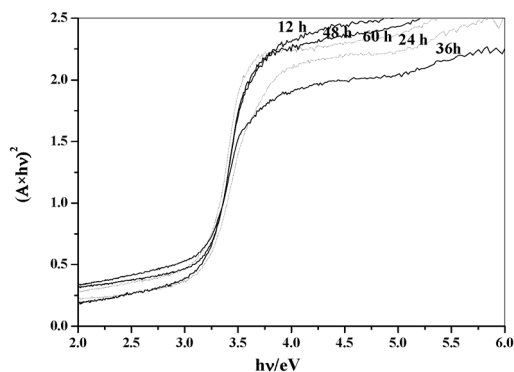


Fig. 4 Graph of samples replotted as $(A \times hv)^2$ vs. (hv) .

Figure 5 shows the PL spectra of the brookite samples (excitation wavelength = 380 nm). It can be seen that the PL emission intensity of sample (36 h) is lower than that of other samples. Since the PL emission is the result of the recombination of excited electrons and holes, the lower PL intensity of the sample (36 h) indicates a lower recombination rate, which is probably the reason for the relatively higher photocatalytic activity.

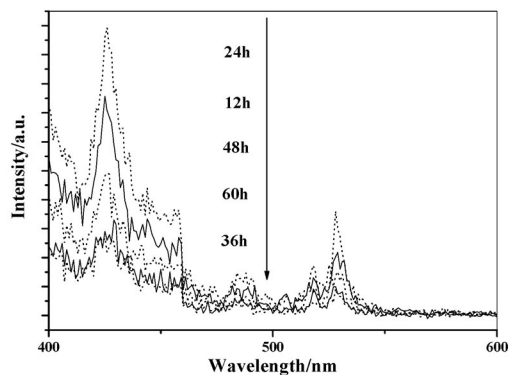


Fig. 5 PL emission spectra for brookite samples.

Figure 6 shows TEM images of brookite particles obtained by the hydrothermal treatment at 24 and 60 h, respectively. All the samples were composed of rod-like nanosized particles. Larger parts were obtained for 60 h sample, indicating that larger particle size would be formed at hydrothermal synthesis time extension. These results are consistent with the XRD patterns.

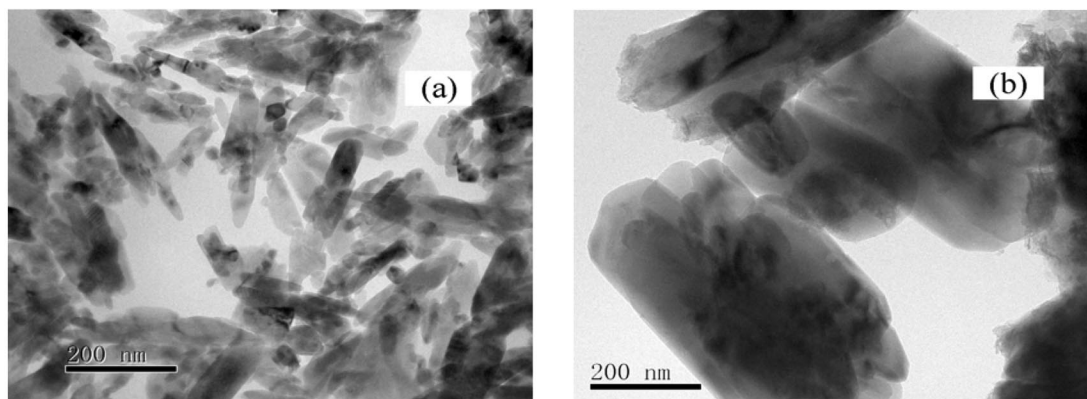


Fig. 6 TEM image of samples prepared at different hydrothermal times (a) 24 h, (b) 60 h.

The photocatalytic activity of brookite samples was investigated by determining the remaining concentration of RhB at various time intervals. Figure 7 is photodegradation ratio of Rh B (10 mg l^{-1}) under iodine tungsten lamp irradiation by different samples. Brookite sample (hydrothermal time 36 h) showed the best photocatalytic activity, and the decolorization efficiency was 91 % after 3 h irradiation. Figure 8 is the UV-vis spectrum of Rh B under sample (hydrothermal time 36 h) for 3 h. During the process of irradiation, the maximum absorption peak shifted gradually from 552 to 498 nm, indicating dissociation of ethyl. The change of characteristic absorption peak is listed in Table 2. Under illumination, the dye was de-ethylated in a stepwise manner with the color of the dispersion changing from initial red to a light green-yellow. De-ethylation of the fully N,N,N',N' -tetraethylrhodamine molecule (i.e., Rh B) has the wavelength position of its major absorption band moved toward the blue region, λ_{max} , Rh B, 552 nm; N,N,N' -triethylrhodamine, 539 nm; N,N' -diethylrhodamine, 522 nm; N -ethylrhodamine, 510 nm; and Rh, 498 nm [22,23]. Rh B formed Rh after being fully demethylated, and the rest was degraded through destruction of the conjugated structure. Results showed that photodecolorization of chromogenic aromatic ring and dissociation of ethyl occurred simultaneously, and the main reaction at the early stage was the photodecolorization of the chromogenic group.

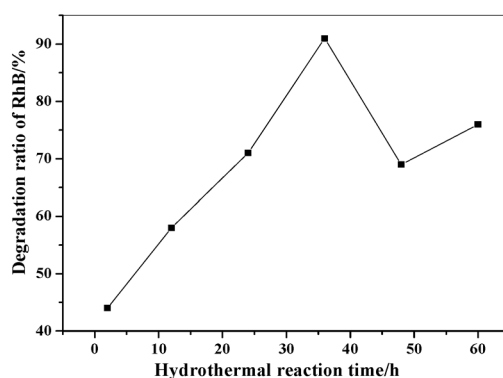


Fig. 7 Photodecolorization ratio of Rh B under different samples.

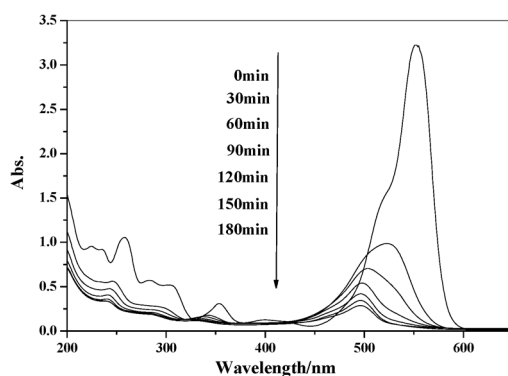


Fig. 8 UV-vis spectrum of Rh B under sample (36 h).

Table 2 Characteristic absorption peaks of de-ethyl compound of Rh B.

Rhodamine B	<i>N,N,N'</i> -triethylrhodamine	<i>N,N</i> -diethylrhodamine	<i>N</i> -ethylrhodamine	Rhodamine
552 nm	539 nm	522 nm	510 nm	498 nm

The reaction mechanism of photodecolorization was further supported by FED. For the hydroxylation reaction, an initial position of OH^\bullet radical attack was estimated from calculation of the FED. The first reaction probably happened on the atom with the highest FED value, which was found higher especially at N29 and N24 atoms (Table 1). Therefore, N29 and N24 should be the first sites at which positions were attacked. Seen from the UV-vis spectroscopy analysis, de-ethylated product was detected. The theoretical analysis is consistent with the experimental results.

CONCLUSION

Phase-pure brookite TiO_2 was prepared by hydrothermal reaction with $\text{Ti}(\text{SO}_4)_2$ as reaction precursor, which is economic and readily achieved. Also, perfect crystalline was obtained even at 180 °C after 24 h. Increasing the hydrothermal time led to better crystalline and larger particle size. Synthesis conditions such as hydrothermal temperature or pH change would be under further consideration, which may lead to interesting results. The catalyst exhibits good heterogeneous activity in photodecolorization of Rh B, the possible decolorization mechanism is proposed not only experimentally but also theoretically by calculating the FED of Rh B. The theoretical analysis is consistent with the experimental results, which explain the hydroxylation reaction product over brookite TiO_2 under illumination.

ACKNOWLEDGMENTS

This work was partly supported by the China Postdoctoral Science Foundation (Grant No. 20070420971), Social Development Foundation of Zhenjiang, China (Grant No. SH2009003), and the Industry High Technology Foundation of Jiangsu Province (Grant No. BG2007025).

REFERENCES

1. H. Kominami, M. Kohno, Y. Kera. *J. Mater. Chem.* **10**, 1151 (2000).
2. M. Anpo. *Pure Appl. Chem.* **72**, 1265 (2000).
3. M. Anpo. *Pure Appl. Chem.* **72**, 1787 (2000).
4. X. M. Lü, J. Liu, J. M. Xie, H. Zhang, Z. J. Gu. *Mater. Sci. Forum* **561–565**, 1089 (2007).
5. J. Liu, X. M. Lü, J. M. Xie, H. Zhang, Z. J. Gu. *Adv. Mater. Res.* **26–28**, 1083 (2007).
6. K. Rajeshwar, C. R. Chenthamarakshan, S. Goeringer, M. Djukic. *Pure Appl. Chem.* **73**, 1849 (2001).
7. N. H. Zhao, L. J. Fu, L. C. Yang, T. Zhang, G. J. Wang, Y. P. Wu, T. V. Ree. *Pure Appl. Chem.* **80**, 2283 (2008).
8. L. J. Fu, T. Zhang, Q. Cao, H. P. Zhang, Y. P. Wu. *Electrochem. Commun.* **9**, 2140 (2007).
9. H. K. Ha, M. Yosimoto, H. Koinuma, B. K. Moon, H. Ishiwara. *Appl. Phys. Lett.* **68**, 2965 (1996).
10. X. Bokhimi, A. Morales, M. Aguilar, J. A. Toledo-Antonio, F. Pedraza. *Int. J. Hydrogen Energy* **26**, 1279 (2001).
11. M. Koelsch, S. Cassaignon, J. F. Guillemoles, J. P. Jolivet. *Thin Solid Films* **403–404**, 312 (2002).
12. W. K. Li, X. Q. Gong, G. Z. Lu, A. Selloni. *J. Phys. Chem. C* **112**, 6594 (2008).
13. S. Bakardjieva, V. Stengl, L. Szatmary, J. Subrt, J. Lukac, N. Murafa, D. Niznansky, K. Cizek, J. Jirkovsky, N. Petrova. *J. Mater. Chem.* **16**, 1709 (2006).
14. W. F. Yan, B. Chen, S. M. Mahurin, V. Schwartz, D. R. Mullins, A. R. Lupini, S. J. Pennycook, S. Dai, S. H. Overbury. *J. Phys. Chem. B* **109**, 10676 (2005).
15. S. Bakardjieva, V. Stengl, L. Szatmary, J. Subrt, J. Lukac, N. Murafa, D. Niznansky, K. Cizek, J. Jirkovsky, N. Petrova. *J. Mater. Chem.* **16**, 1709 (2006).
16. SDK News Release 2005, <<http://www.products-e.sdk.co.jp/SDK/products-e/products-e.nsf/fc44548239ff752849257185001e45bf/85f454052b12342a492572800011cd3c!OpenDocument>>.
17. K. Tomita, V. Petrykin, M. Kobayashi, M. Shiro, M. Yoshimura, M. Kakihana. *Angew. Chem., Int. Ed.* **45**, 2378 (2006).
18. H. Kominami, M. Kohno, Y. Kera. *J. Mater. Chem.* **10**, 1151 (2000).
19. M. Kobayashi, K. Tomita, V. Petrykin, S. Yin, T. Sato, M. Yoshimura, M. Kakihana. *Solid State Phenom.* **124–126**, 723 (2007).
20. N. Murakami, T. Kamai, T. Tsubota, T. Ohno. *Catal. Commun.* **963–966**, 10 (2009).
21. M. J. Frisch, G. W. Trucks, H. B. Schlegel et al. Gaussian (Revision C. 02), Gaussian, Inc., Wallingford, CT.
22. T. Watanabe, T. Takizawa, K. Honda. *J. Phys. Chem.* **81**, 1845 (1977).
23. T. Inoue, T. Watanabe, A. Fujishima, K. Honda, K. Kohayakawa. *J. Electrochem. Soc.* **124**, 719 (1977).